Elaboration of the structural and physical characteristics: Ni-doped ZnO bulk samples prepared by solid state reactions

G. BULUN[a], A. EKICIBIL[a*], S. K. CETIN[a], S. DEMİRDİS[c], A. COSKUN[b], K. KIYMAC[a]
[a]*Department of Physics, Faculty of Sciences and Letters, Cukurova University, 01330 Adana, Turkey*
[b]*Department of Physics, Faculty of Sciences and Letters, Mugla University, 48000, Mugla, Turkey*
[c]*Laboratoire des Solides Irradiés, Cnrs-Umr 7642&Cea/Dsm/Iramis, Ecole Polytechnique,F 91128, Palaiseau cedex, France*

Ni-doped ZnO ($Zn_{1-x}Ni_xO$, with $0.25 \leq x \leq 0.50$) diluted magnetic semiconductors were prepared by the solid state reaction method. We have studied the structural properties of the samples by using the X-Ray Diffraction (XRD), Scanning Electron Microscopy (SEM), Atomic Force Microscopy (AFM) and Energy Dispersive X-Ray spectroscopy (EDX) techniques. The SEM and AFM results clearly demonstrate that Ni^{2+} ions integrate into the ZnO structure without any problem. The grains of the samples are very well connected to each other and tightly packed, and vary in size from 0.2μm to 2μm. From the XRD and EDX spectra of the samples, it has been concluded that the doping causes no change in the hexagonal wurtzite structure of ZnO. However, the XRD indicated that three additional peaks, related to the (102),(012) and (108) planes appeared for the doped samples. Furthermore, an additional NiO-associated diffraction peak appears for the highest concentration of Ni, i.e., for x=0.50 of Ni^{2+} doping, which indicates an upper limit for Ni concentration. The estimated crystal sizes from the XRD results vary from 4.38 Å to 9.73 Å. The lattice parameter *a* and *c* of Ni-doped ZnO are slightly smaller and higher than that of pure ZnO, respectively. These observations may be due to the slightly different ionic sizes of Zn^{2+} and Ni^{2+} ions.

(Received March 14, 2011; accepted March 21, 2011)

Keywords: ZnO, AFM, XRD, SEM, Semiconductors, EDX, Ni-doped ZnO

1. Introduction

Diluted magnetic semiconductors (DMS), in general, exhibit simultaneously both ferromagnetic and semiconducting properties. They are prepared by entering magnetic atoms or ions in to solid solutions of semiconducting host materials. Doped semiconductors show different magnetic behaviors, depending upon the concentration of magnetic elements, synthesis route and experimental conditions [1]. Currently, ZnO-based magnetic semiconductors have been attracting a great deal of attention for their potential applications in spintronics materials and for the important optoelectronic properties of ZnO at practical temperatures [2-7]. It has been theoretically predicted that, when suitably doped with transition metal ions (Ni, Mn, Co, V or Fe), ZnO could be made to be ferromagnetic with Curie temperatures (T_c) higher than the room temperature [8-9]. At room temperatures, ferromagnetism (FM) has been predicted in Mn-doped p-type ZnO by Dietl et al. [8-10]. Dietl et al. considered GaN and ZnO as candidates causing a high T_c and a large magnetization, when doped with transition metal ions. Sato et al. [9] suggested theoretically that the ferromagnetic state in Mn, Fe, Co and Ni-doped ZnO, a DMS, can be stabilized. The first principle calculations [11] based on density functional theory (DFT) also predict ferromagnetism in most 3d transition metal (TM) doped ZnO, which make ZnO one of the most promising material in spintronics, and therefore, there is a growing interest in this material, recently. Furthermore, ZnO, being II-VI or III-V semiconductor compound with a wide band gap of about 3.4 eV, is an attractive material for applications in optical devices, such as, blue, violet and UV light emitting diodes (LEDs) and laser diodes (LDs). ZnO is also a strong piezoelectric material. Thus, the transition metal doped ZnO materials are expected to be highly multifunctional materials with coexisting magnetic, semiconducting, electromechanical and optical properties. After the theoretical works, predicting room temperature ferromagnetism in ZnO doped with transition metals [12-16], intensive efforts were expended on ZnO thin films doped with Mn, Co etc. [17-18]. The experimental results, however, have not converged on a definite conclusion; rather conflicting observations were reported by different groups for both Co-doped [17] and Mn-doped ZnO thin films [18]. These disagreements suggest a possibility that the films investigated in the reported works may have different small scale structures, despite the fact that, they all shared the same Bragg peaks. Since these structures could not be easily detected in thin films with usual x-ray diffraction (XRD), we believe that careful structural and magnetic investigations on bulk samples are desired to

resolve the controversy. It should be pointed out that a reasonably high solubility of TM in ZnO allows this type of investigations to be done.

Therefore, in order to test our predictions, in this work we present our studies on Ni-doped ZnO prepared by the solid state reaction technique. The solid state reaction is chosen because of its reproducibility, easy control and sufficient products needed for measurement. We have compared the structural properties of un-doped ZnO and Ni-doped ZnO ($Zn_{1-x}Ni_xO$) with $0.25 \leq x \leq 0.50$, by using various methods, such as, X-Ray Diffraction (XRD), Scanning Electron Microscope (SEM), Atomic Force Microscope (AFM) and Energy Dispersive X-Ray Analysis (EDX).

2. Experimental procedure

In the present investigation, the polycrystalline samples of $Zn_{1-x}Ni_xO$ (x= 0.25, 0.30, 0.35, 0.40, 0.45, 0.50) were synthesized by the standard solid state reaction method. The raw materials were pure ZnO and NiO powders which are known to be non-ferromagnetic. In the solid state reaction route appropriate amounts of ZnO and NiO were mixed and ground in an agate mortar. The resulting powders were calcined at 350 °C for 4h in air, and thereafter they were furnace cooled. After cooling, the resulting materials were reground and pelletized using a cylindrical die of 10 mm in diameter, under a pressure of 20 bars. Finally all the pellets were heat treated at 950 °C in air for 24h, and were then furnace cooled to the room temperature.

The $Zn_{1-x}Ni_xO$ samples, prepared as explained above, were characterized by x-ray diffraction (XRD), (Phillips X'Pert Pro, with wavelength of 1.54 Å in the wide angle region from 25° to 70° on 2θ scale) and energy dispersive x-ray (EDX), (Phillips XL-3DSFEG), in order to elaborate structural properties in a precise manner for various doping concentration of Ni. The surface morphologies and grain sizes of the prepared samples were found using a scanning electron microscope (SEM), (Philips XL-3DSFEG), and an atomic force microscope (AFM), (Solver-PRO). For the differential thermal analysis (DTA) and thermal gravity analysis (TGA) investigations, 10mg well grained powders of each sample were examined from room temperature to 1300 °C, at a heating rate of 10 °C/min with Perkin Elmer-Diamond system.

3. Results and discussion

The thermal behaviors of the sample with x=0.50, obtained by DTA and TGA analysis, are shown Figs.1a and 1b, respectively. The DTA curve of the sample shown in Fig.1a demonstrates two endothermic peaks; one at about 920 °C and the other at 1080 °C. Therefore, it's clear that before the crystallization peak temperature, endothermic activities occurred at these temperatures. On the other hand, two exothermic peaks also appeared at about 1050 and 1350 °C. Figure-1b illustrates the TGA curve of the x=0.50 sample during the heating process. The related weight loss, between the endothermic peak occurring just above 1269°C and the exothermic peak at about 1440°C, arises from the evaporation and combustion. The total weight loss is about 23%. These results have leaded us to heat treat our samples at 950 °C, as stated in the previous section.

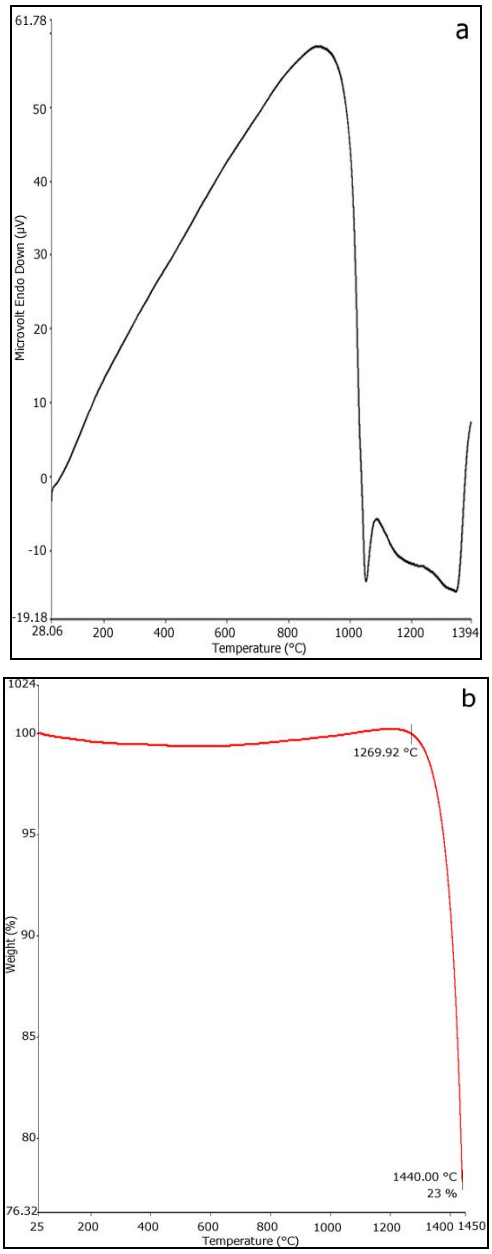

Fig. 1. DTA (a) and TGA (b) curves of the sample x=0.50 taken at heating rate of 10 °C/min

The XRD technique was used to characterize the structure of the powdered products. The x-ray powder diffraction (XRD) patterns of the as-synthesized samples without and with different amounts of Ni in $Zn_{1-x}Ni_xO$ are presented in Fig. 2. Among the XRD patterns of Figure-2, nine strong peaks appear, for all the concentrations, at

about $2\theta \approx 32°$, 34°, 36°, 37°, 43°, 48°, 57°, 63° and 68° which correspond to the reflected intensity from the (100), (002), (101), (102), (012), (102), (110), (103) and (112) planes of the hexagonal structure of ZnO, respectively. The XRD spectra show broad peaks at these positions, which are apart from the peaks at 2θ=37°, 43° and 63° in the (102), (012) and (103) planes (that are missing for the pure ZnO), in good agreement with the standard JCPDS file for ZnO, and can therefore be indexed as the hexagonal wurtzite structure of ZnO having space group $P6_{3mc}$. Therefore, one can point out that the XRD results indicate the presence of additional phases (planes), such as, (102), (012) and 103), in the Ni-doped samples. On the whole, after partial substitution of Zn by Ni, the diffraction patterns for all the samples show almost the same peaks, which indicates that the wurtzite structure is not disturbed by Ni substitution, and a uniform doping throughout the samples is achieved. As a result the x-ray powder diffraction patterns of Ni-doped ZnO samples are almost the same as that of pure ZnO and thus can be identified as having the wurtzite structure, nearly the same as that of ZnO. No diffraction lines of NiO are observed for Ni concentrations with $x \leq 0.45$. However, when x was increased to 0.50, the NiO (200) peak could be clearly seen in the XRD pattern of $Zn_{0.5}Ni_{0.5}O$ (as denoted by an arrowhead in Fig.2). This new phase in the XRD spectra corresponding to NiO (200) may be due to the formation of NiO from remaining un-reacted Ni^{2+} ions present in the solutions. That's to say that, phase segregation has started in this system and the solubility of Ni in $Zn_{1-x}Ni_xO$ (x=0.50) has decreased. We should point out that the peaks in the diffraction patterns of doped samples are slightly shifted to lower or higher angles as compared to the pure ZnO. For example, the position of the XRD peak corresponding to the (102) plane is seen to be shifted first towards upward i.e., to 2θ=36.00°, 36.31°, 36.47° with increasing Ni content up to x=0.30, and then shifted towards downward, i.e., to 2θ=35.91°, 36.08°, 36.01°, 36.27° with increasing Ni content up to x=0.50. This means that small variations in the lattice parameters occur as the Ni concentration increases. The d(102) values obtained from these peaks are plotted as a function of Ni content in the inset of Figure-2. As seen the lattice spacing d(102) first increases linearly with increasing Ni content up to x=0.40; indicating that Ni ions are substituted for Zn ions in ZnO without changing the wurtzite structure. Thus, nickel ions can be uniformly doped into wurtzite ZnO by replacing the zinc sites. The small difference between the ionic radii of the tetrahedrally coordinated zinc(II) (0.74Å) and the nickel(II) (0.68Å) allows incorporation of Ni^{2+} into ZnO with only a slight decrease in the lattice parameters *a* and a slight increase in lattice parameters *c* that cause a small shift of all the peaks to lower or higher angles. Calculations on the basis of the XRD patterns show that ZnO powder has a polycrystalline hexagonal wurtzite crystal structure with *a*=3.2448Å, *c*=5.2194Å and V=54.9536 $Å^3$. Table-1 shows that the lattice constants *a* and *c* of $Zn_{1-x}Ni_xO$ are in general, slightly lower and higher than those of the pure ZnO, respectively. These variations are certainly related to the fact that as indicated above the ionic radius of Zn^{2+} is larger than that of Ni^{2+}. The slight reduction of the lattice constants *a* of $Zn_{1-x}Ni_xO$ indicates that nickel is really, at least partially, integrates into the ZnO structure. It should also be pointed out that a strong correlation exists between the *c/a* ratio and the *u* parameter, when the *c/a* ratio increases, the *u* parameter should decrease in such way that those four tetrahedral distances remain nearly constant through a distortion of tetrahedral angles due to long-range polar interactions. Our data in Table-1 confirm these statements (compare the *c/a* and *u* columns). In other words, Table-1 shows that, as expected, there is a slight decrease in the *u* parameter and a slight increase in the *c/a* ratio with increasing Ni content. These two slightly different bond lengths will be equal if the following relation holds [19]:

$$u=(1/3)(a^2/c^2)+1/4$$

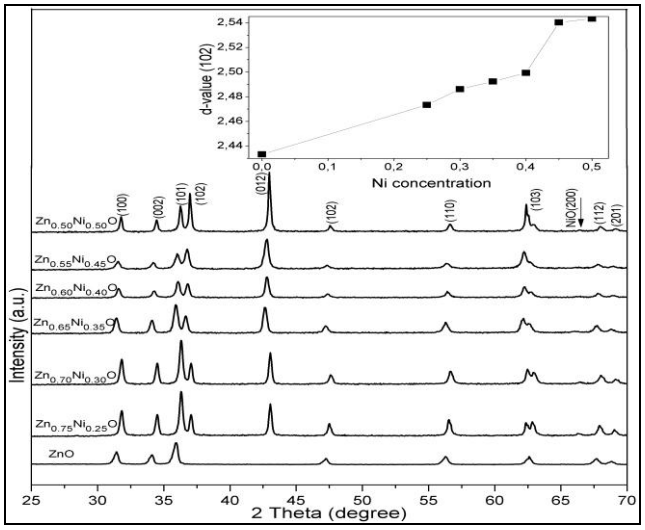

Fig. 2. XRD patterns of $Zn_{1-x}Ni_xO$ for all concentrations. The insert shows the d-values versus Ni concentrations.

Since the *c/a* ratio also correlates with the difference of the electronegativities of the two constituents, components with the great differences such as those with concentrations of x=0.45 and x=0.50, show the largest departure from the ideal *c/a* ratio. The sizes of the crystals in the heat treated pellets (samples) may be roughly calculated by using the following relation known as Scherer's equation:

$$D_{h,k,l} = \kappa\lambda / (B\cos\theta) \quad (1)$$

where D is the particle size, λ the wavelength of x-ray radiation used (1.54 Å), θ the Bragg angle, B is the full-width at half-maxima (FWHM) on 2θ scale and κ is 0.9. By using the above relation the crystalline sizes were evaluated for the strongest x-ray diffraction, corresponding to the (101) peaks at 36.29º, and were found to vary from 4.38 Å to 9.73 Å for all the samples (see the last two columns of Table-1).

Table 1. Nominal compositions and structural parameters of $Zn_{1-x}Ni_xO$.

Samp.	Ni content, x	Lattice parameters for the $Zn_{1-x}Ni_xO$		Unit cell volume, ($Å^3$)	c/a	u	FWHM	θ (Degr)	D(Å)
		a (Å)	c (Å)						
ZnO	0.00	3.2448	5.2194	54.9536	1.6084	0.3788	0.2598	35.9831	6.5952
A	0.25	3.2200	5.2179	54.1013	1.6204	0.3769	0.1948	36.1976	8.8200
B	0.30	3.2121	5.1970	53.6205	1.6179	0.3773	0.2273	36.3219	7.5710
C	0.35	3.2408	5.2571	55.2142	1.6221	0.3767	0.3897	35.9323	4.3841
D	0.40	3.2340	5.2361	54.7631	1.6190	0.3772	0.2598	42.7512	7.2679
E	0.45	3.2304	5.2509	54.7957	1.6254	0.3762	0.2598	42.8220	7.2763
F	0.50	3.2301	5.2504	54.7802	1.6255	0.3761	0.1948	42.9589	9.7258

The SEM and AFM techniques were employed to explore the sizes and distributions of the particles in the materials. A comparison of the SEM images of the samples revealed that particles (grains) are more closely packed and have smaller sizes with increasing nickel concentrations. Furthermore the grains are nearly oval and spheroidal shaped for all the samples. As an example Figure-3 shows SEM images as well as the corresponding energy dispersive x-ray (EDX) spectra of the $Zn_{1-x}Ni_xO$ samples with x=0.25 and 0.50. From the similarity of the Zn and Ni peak intensity line traces in EDX spectra of the samples, it is concluded that after the synthesis process, zinc and nickel were almost homogenously distributed throughout the samples. In other words, the EDX line traces indicate that Ni^{2+} was successfully integrated into the crystal structure of ZnO. All the locations contain the expected elements (Zn, Ni, O), and no other impurity elements are detected. For the samples with x=0.25 and 0.50 the quantitative elemental distributions, in atomic percentage of Zn, Ni and O, obtained from EDX are presented in Table -2.

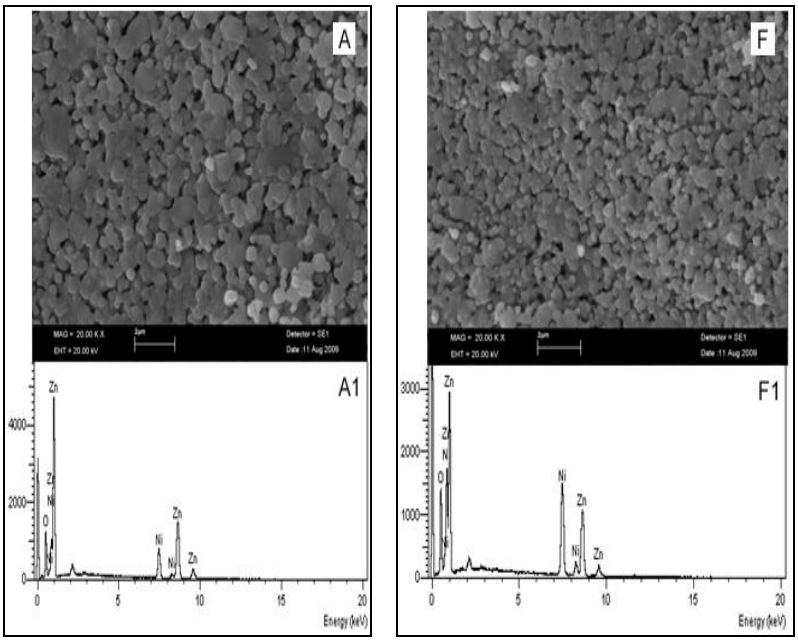

Fig. 3. SEM (A), (F) images, and EDX (A1), (F1) spectra of $Zn_{1-x}Ni_xO$, indicating the elemental distribution in A) x=0.25 and F) x=0.50.

Table 2. The quantitative elemental distribution in atomic Percentage of Zn, Ni and O elements for A (x=0.25) and F (x=0.50).

Elements	Atomic Percentage (%)	
	A (x=0.25)	F (x=0.50)
O	45.96	48.66
Zn	42.78	28.90
Ni	11.26	22.44

In order to investigate and compare the surface morphologies of the non-doped and the doped samples, apart from the SEM images, the AFM images with a scan area of 20 μm x 20 μm are also taken in contact mode and shown in Figures 4A-F. Each set of figures contain 2-D (on the left side) and 3-D (in the middle) surface topographies and the line (on the right side) profiles. The AFM images, shown in a 3-D, give informations about what the surface topography actually looks like.

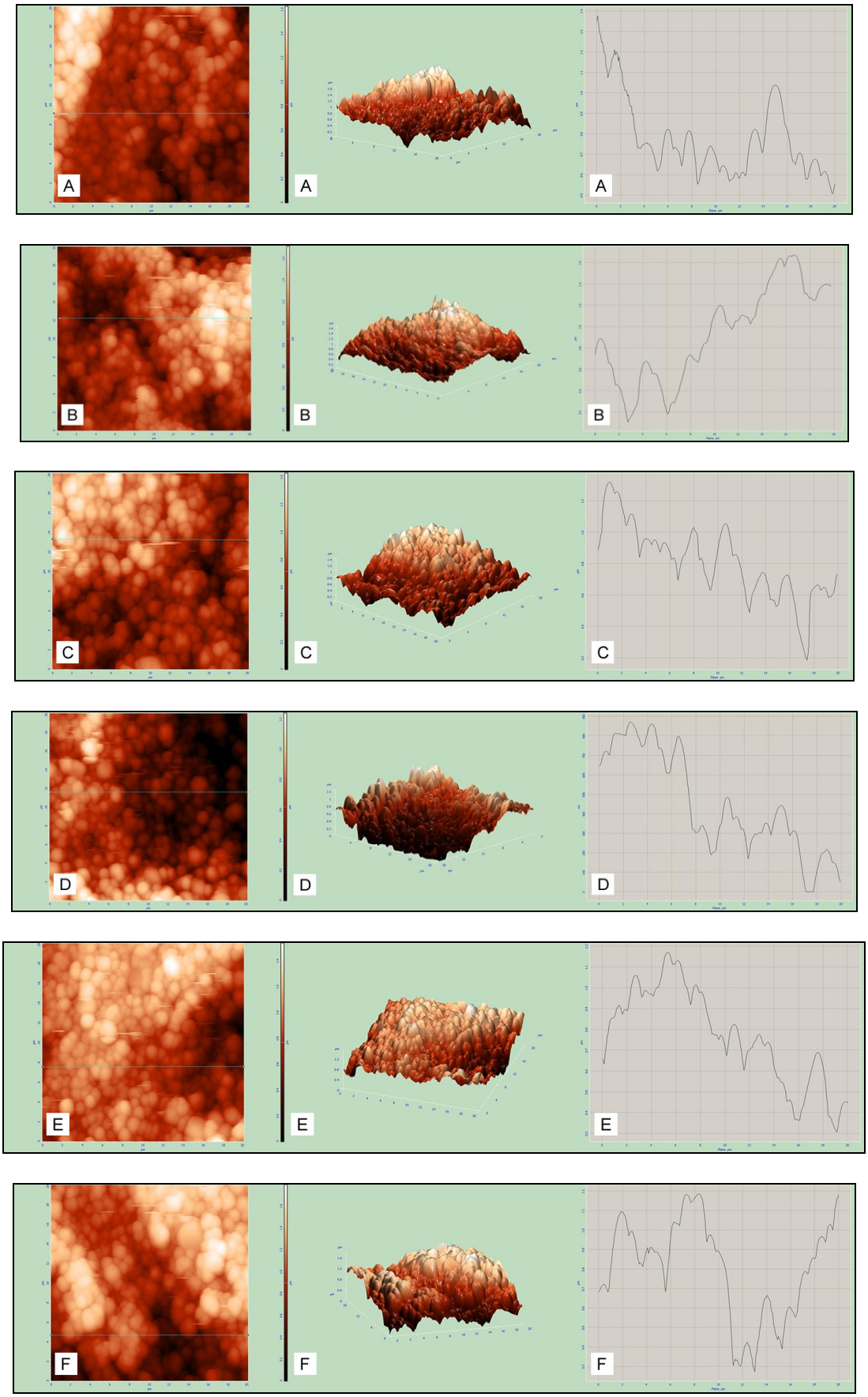

Fig. 4. AFM images of precursor materials $Zn_{1-x}Ni_xO$ for $0.00 \leq x \leq 0.50$.

It is clearly seen from the images in Figs.4, that the non-doped sample has larger grain sizes than those of the doped samples. These grains are well connected to each other and tightly packed, in agreement with SEM images. Average grain sizes of non-doped sample are in between 0.5-2μm. As a result of Ni ions entering into the structure, average grain sizes decrease somewhere in between 0.2-1μm, this trend is also in quite good agreement with the SEM, as well as with the X-Ray results. However, it is obvious from the 3-D AFM images, that the doped samples have rougher surface morphologies. These rough surfaces observed in the doped samples may arise from ionic radius differences of the Ni (0.69 Å) and Zn (0.74 Å) ions. A comparison of the line profiles indicates that the grain sizes of the doped samples decrease compared to those of the non-doped sample, again in agreement with the SEM and AFM images.

4. Conclusions

In summary, Ni-doped ZnO ($Zn_{1-x}Ni_xO$, $0.00 \leq x \leq 0.50$) diluted magnetic semiconductor samples are prepared by the so called solid state reaction method. From the structural analysis of the samples explored by XRD and EDX techniques, it has been concluded that almost no change in the wurtzite structure of ZnO is observed for the nickel concentration levels studied in this work. The XRD, SEM and AFM results indicate that all of the powdered $Zn_{1-x}Ni_xO$ samples are polycrystalline, with a mean size lying in the sub-micrometer range, for $0.25 \leq x \leq 0.50$. Furthermore, SEM, EDX and AFM results clearly demonstrate that Zn^{2+} ions are easily replaced by Ni^{2+} ions, that is, Ni can be homogenously distributed in ZnO matrix, for $x \leq 0.50$.

Acknowledgements

This work is supported by the Research Fund of Çukurova University, Adana, Turkey, under grant contracts no. FEF2009BAP10, no. AMYO2009BAP1, no. FEF2005. D16. We wish to thank Aydin Eraydin for his help.

References

[1] T. Dietl, Semicond. Sci.Technol.**17**, 377 (2002).
[2] S.A. Wolf, P.Treger, IEEE Tran.Magn. **36**, 2748 (2000).
[3] S. A. Wolf, D. D. Awschalon, R. A. Buhrman, J. M. Daughton, S. von Molnar, M. L. Roukes, A. Y. Chtchelkanova, and D.M.Treger, Science **294**, 1488 (2001).
[4] H. J. Lee, S. Y. Jeong, C. R. Cho, C. H. Park, Appl. Phys. Lett. **81**, 4020 (2002).
[5] J. M. D. Coey, A. P. Douvalis, C. B. Fitzgerald, M. Venkatesan, Appl. Phys. Lett. **84**, 1332 (2004).
[6] K. Ueda, H. Tabata, T. Kawai, Appl. Phys. Lett. **79**, 988 (2001).
[7] I. H. Karahan, A. Ekicibil, Optoelectron. Adv. Mater. Rapid. Commm. **11**, 722 (2008).
[8] T. Dietl, H. Ohno, F. Matsukura, J. Cibert,, D. Ferrand, Science **287**, 1019 (2000).
[9] K. Sato, H. Katayama-Yoshida, Jpn. J. Appl. Phys.,Part2, **39**, L555 (2000).
[10] T. Dietl, J. Appl. Phys. **89**, 7437 (2001).
[11] Sluiter MHF, Kawazoe Y, Sharma P, Inoue A, Raju AR, Rout C, Waghmare UV, Phys. Rev. Lett. **94**, 187204 (2005).
[12] P. Sharma, A. Gupta, K. V. Rao, F. J. Owens, R. Sharma, R. Ahuja, J. M. Osorio Gullen, B. Johansson, and G. A. Gehring, Nature Material **2**, 673 (2003).
[13] D.C. Kundaliya, S.B. Ogale, S.E. Lofland, S. Dhar, C. J. Metting, S. R. Shinde, Z. Ma, B. Varughese, K. V. Ramanujachary, L. Salamanca-Riba, T. Venkatesan, Nature Material **3**, 637 (2004).
[14] T. Fukumura, Z. Jin, A. Ohtomo, H. Koinuma, M. Kawasaki, Appl. Phys. Lett. **75**, 3366 (1999).
[15] Sang-Wook Lim, Min-Chang Jeong, Moon-Ho Ham, Jae-Min Myoung, Jpn. J. Appl. Phys. **43**, L280 (2004).
[16] S. W. Jung, S. J. An, G. C. Yi, C. U. Jung, S. Lee, S. Cho, Appl. Phys. Lett. **80**, 4561 (2002).
[17] Z. Jin, T. Fukumura, M. Kawasaki, K. Ando, H. Saito, T. Sekiguchi, Y.Z. Yoo, M. Murakami, Y. Matsumoto, T. Hasegawa, H. Koinuma, Appl. Phys. Lett. **78**, 3824 (2001).
[18] T. Fukumura, Z. Jin, M. Kawasaki, T. Shono, T. Hasegaw, S.Koshihara, H. Koinuma, Appl. Phys. Lett. **78**, 958 (2001).
[19] U. Ozgur, Ya. I. Aliov, C. Liu, A. Teke, M. A. Reshchikov, S. Dogan, V. Avrutin, S. J. Cho, H. Markoc, Applied Physics Reviews, **98**, 041301 (2005).

*Corresponding author: ahmetcan@cu.edu.tr